https://doi.org/10.5194/egusphere-2026-3817
Preprint. Discussion started: 14 July 2026

Contribution of stratospheric intrusion to tropospheric hydroxyl radical

Zhiting Wang[1], Yijie Zheng[1], Xinlong Hong[1], Plummer David[2], Jun Zhang[3]

[1]College of Atmospheric Sciences, Lanzhou University, Lanzhou 730000, China

[2]Climate Research Division, Environment and Climate Change Canada, Montréal, Canada

[3]NSF National Center for Atmospheric Research, Boulder, CO, USA

Correspondence: Z. Wang (wangzt@lzu.edu.cn)

Abstract

The hydroxyl radical (OH) is a key species that participates in many oxidation processes in the troposphere. Previous studies have reveal significant impact of lightning and air pollution on interannual variabilities and long-term trends of tropospheric OH. The abundance of OH in the troposphere is influenced by a multitude of factors, including ozone, water vapour, and ultraviolet radiation, among others. The tropospheric ozone is significantly influenced by the presence of stratospheric intrusion. It is hypothesized that the intrusion process will also exert an influence on tropospheric OH. In this study, the contribution of stratospheric intrusion to tropospheric OH is estimated through the use of a climate chemistry model. The findings suggest that the contribution of the stratosphere to tropospheric OH is most significant over the subtropical ocean regions (reaching 2×10^{-2} ppt) and over the Tibetan Plateau in the summer (reaching 3×10^{-2} ppt). The relative contribution of stratospheric intrusion can reach 12% over the Tibetan Plateau, northern South America and South Africa, and 20% over the subtropical oceans. It is expected that stratospheric contribution will increase in the future due to enhanced stratosphere troposphere exchange and stratospheric ozone recovery.

Keywords: stratospheric intrusion; ozone; tropospheric hydroxyl radical

1 Introduction

Hydroxyl radicals (OH) are critical oxidants in the atmosphere, playing a vital role in controlling the concentrations of pollutants and greenhouse gases (Levy, 1971). Consequently, these radicals impact both air quality and climate change. Therefore, a comprehensive understanding of the

https://doi.org/10.5194/egusphere-2026-3817
Preprint. Discussion started: 14 July 2026

sources, distribution, and reactivity of OH is essential for atmospheric chemistry and its ramifications for human health and the environment. Research on OH radicals has a long history, evolving from early discoveries of atmospheric free radicals to sophisticated measurements using techniques like Laser-Induced Fluorescence (LIF) and modelling approaches (Spivakovsky et al., 2000; Montzka et al., 2011; Rigby et al., 2017; Turner et al., 2017). The primary production of OH is through the reaction of water vapour with excited oxygen atoms $O(^1D)$, which are generated by ozone (O_3) photolysis (λ<340 nm). Secondary sources of OH include the recycling of HO_2 by reaction with NO. As posited by Lelieveld et al. (2016) the primary production contributes approximately 33% of the tropospheric OH, while secondary sources contribute approximately 30%. In the troposphere, the lifetime of OH is short, measured in mere seconds, due to its rapid removal by reactions with carbon monoxide (CO), methane (CH_4) and non-methane volatile organic compounds (NMVOCs). The prevalence of OH is indicative of the confluence of atmospheric composition (tropospheric O_3 and NO, CO, CH_4 and NMVOCs) and meteorological factors (e.g., humidity, ultraviolet radiation, and temperature).

Direct measurements of OH are challenging due to its short lifetime. Presently, the spatial distribution and temporal trends of OH are estimated indirectly through the measurement of CH_3CCl_3, which is primarily removed through an oxidation reaction with OH. However, discrepancies have been observed between the interannual variabilities of tropospheric OH as simulated by atmospheric models and the indirect estimation. For instance, indirect estimations generally indicate a peak in OH abundance around 2004, which can account for the nearly constant mixing ratios of tropospheric methane from 1997 to 2006 and the increasing ratios before and after this period. However, this peak in OH abundance was not present in models (Nicely et al., 2018; Patra et al., 2020). According to Nicely et al. (2020), the predominant factors contributing to variations in tropospheric oxidation capability among 10 models are the flux of ultraviolet radiation to the troposphere, the mixing ratio of tropospheric O_3, the abundance of nitrogen oxides (NO_x), and the complexity of the various chemical mechanisms that drive OH. Furthermore, the presence of water vapour and carbon monoxide, the ratio of NO:NO_x and formaldehyde (HCHO) contributes to moderate variations. The extensive array of factors underscores the complexity of constraining tropospheric OH.

There is significant interaction between the stratosphere and the troposphere, particularly along the subtropical jet streams. Planetary-scale waves propagate and break along these streams, resulting in a folded tropopause and the downward intrusion of stratospheric air. These events usually transport ozone-rich air into the troposphere and consequently alter its composition. Stratospheric intrusions,

https://doi.org/10.5194/egusphere-2026-3817
Preprint. Discussion started: 14 July 2026

for example, have the potential to increase surface ozone concentrations and affect air quality (Lin et al., 2015; Knowland et al., 2017). Previous studies have shown that chemical evolution can be sensitive to mixing resulting from stratosphere-troposphere exchange. Using a two-box model, Esler et al. (2001) demonstrated that mixing of stratospheric ozone with tropospheric water vapour leads to increased hydroxyl radical concentrations. When NO_x levels in either parcel are initially very high, the mixing of NO_x becomes more important than ozone and water vapour in determining OH levels. Kentarchos et al. (2003) apply the European Centre Hamburg Model version 4 (3.75°×3.75°, 19 levels) to study the contribution of stratospheric ozone to tropospheric OH. In this model, stratospheric ozone is represented by an ozone potential vorticity correlation. In the troposphere, stratospheric ozone produces OH through photolysis and the subsequent reaction of the resulting $O(^1D)$ with water vapour. Zhang et al. (2024) observed that, during stratospheric air intrusion events, the mixing of descending ozone-rich stratospheric air with more moist free tropospheric air results in elevated OH concentrations.

This study examines the role of stratospheric intrusion in determining tropospheric OH concentrations. For this investigation, the Geophysical Fluid Dynamics Laboratory's AM3 chemistry-climate model was used. This model has a more detailed OH chemistry compared to the previous study. A tagged tracer was used to characterize the stratospheric contribution to tropospheric O_3 abundances. OH radical concentration due to stratospheric intrusion was identified by first removing the stratospheric contribution to tropospheric O_3 and then calling the model's chemical solver with the corrected O_3. The second section describes the model and method utilized. The next section presents the results, which are then discussed. Section 4 draws conclusions.

2 Data and methodology

2.1 Model Description

This study utilizes the Geophysical Fluid Dynamics Laboratory (GFDL) AM3 chemistry-climate model (Donner et al., 2011) to simulate atmospheric O_3 and OH radicals. AM3 implements a cubed-sphere horizontal grid with approximately global uniform grid cell size (Putman & Lin, 2007). The dynamical core is based on the finite-volume transport algorithm with a vertically Lagrangian discretization (Lin, 2004). Each vertical layer evolves separately in a Lagrangian manner, which means the finite volumes bounded by two coordinate surfaces (initial coordinate surfaces are treated as material surfaces) are free vertically to float, compress or expand with the flow as dictated by the hydrostatic dynamics. These vertical layers are only remapped to the normal vertical coordinates in a time step same as the physical parameterization in the model.

https://doi.org/10.5194/egusphere-2026-3817
Preprint. Discussion started: 14 July 2026

In this study, the interactive tropospheric and stratospheric chemistry of AM3 as described in Naik et al. (2013) is replaced with that described in Horowitz et al. (2020). The updated chemistry include heterogeneous reactions of HO_2, NO_2, N_2O_5, and NO_3 on the surfaces of all simulated aerosol types, as described in Mao, Horowitz, et al. (2013) and Mao, Paulot, et al. (2013). The updated heterogeneous chemistry has a stronger sink of HO_2 than that in AM3 and simulates a lower OH concentration in the troposphere. The gamma values applied is the same those in Table S3 of Horowitz et al. (2020).

The deep convection parameterization applied in the AM3 is the one described by Donner (1993, 2011). The closure of this parameterization is based on the relaxation of the CAPE (convective available potential energy) toward a reference value over a specified time scale. The original deep scheme produces air properties in the tropical upper troposphere that are too close to those of the lower troposphere, indicating that the simulated convection is too strong. In this study, the rising air parcel is allowed to be diluted by environmental air during the calculation of CAPE. The entrainment rate is set to $\varepsilon_0/(1+z\varepsilon_0)$, where $\varepsilon_0 = 0.5\times10^{-3}$ m^{-1} is the entrainment rate near the surface and z is altitude in meters. This is larger than the 0.25×10^{-3} m^{-1} used in Cui et al. (2021) and smaller than the 0.7×10^{-3} m^{-1} used in Xie et al. (2019). Here, the value of ε_0 is determined according to the simulated tropospheric OH concentration. The dilution of the rising air parcel will increase sensitivity of simulated convection activity to atmospheric sates. According to Suhas et al. (2014), diluted CAPE improves the simulation of deep convection compared with CAPE closure.

The applied configuration of the AM3 has a horizontal resolution of approximately 100 km (C96) and 64 vertical layers extending from the surface to approximately 86 km. Two artificial tracers, $O_{3,s}$ and $O_{3,rm}$, are defined to quantify the stratospheric influence. These tracers are analogous to atmospheric O_3 above the tropopause. In the atmospheric layer beneath the tropopause, the tracer $O_{3,rm}$ is defined by subtracting $O_{3,s}$ from tropospheric O_3 at each time step. The tracer $O_{3,s}$ is set to zero in the troposphere at each time step. Then, the chemical solver is called again with O_3 replaced by $O_{3,rm}$ to obtain another hydroxyl radical tracer, OH_{rm}, and the chemical tendency of $O_{3,rm}$. Additionally, $O_{3,rm}$ undergoes atmospheric transport and dry deposition similarly to O_3. Stratospheric contributions to tropospheric ozone and hydroxyl radical mixing ratios are estimated as $[O_3]$-$[O_{3,rm}]$ and $[OH]$-$[OH_{rm}]$. Hereafter, these contributions are referred to as $StrO_3$ and StrOH, respectively.

In order to understand the driving factors behind the seasonal variation of StrOH, we calculate the production rate of StrOH due to the photolysis of $StrO_3$ and its reaction with HO_2 as following (Brauers et al., 1998),

https://doi.org/10.5194/egusphere-2026-3817
Preprint. Discussion started: 14 July 2026

$$P(StrOH) = 2f[StrO_3] \times j(O^1D) + k_{O_3+HO_2}[StrO_3][HO_2], \quad (1)$$

where $j(O^1D)$ is the photolysis rate coefficient of ozone and

$$f = \frac{k_{O^1D+H_2O}[H_2O]}{k_{O^1D+H_2O}[H_2O] + k_{O^1D+N_2}[N_2] + k_{O^1D+O_2}[O_2]}. \quad (2)$$

The first term on the right-hand side of Eq. 1 represents the production of OH through the photolysis of $StrO_3$ and the subsequent reaction of $O(^1D)$ with a H_2O molecule to produce 2 OH molecules. Since $O(^1D)$ can transform into O through reactions with N_2 and O_2, the factor f in Eq. 2 is included. The OH loss (sink) is quantified by the first-order loss rate coefficient given by $L(OH)/[OH]$, where $L(OH)$ indicates the loss rate of OH radicals in the troposphere.

In the simulations, AM3 is forced by observed sea surface temperatures (SST) and sea ice concentration (SIC), but horizontal winds are nudged to 6-hourly ERA-Interim reanalysis data (The fourth-generation atmospheric reanalysis developed by the European Centre for Medium-Range Weather Forecasts), which has a horizontal resolution of 2.5°×2.5°. A pressure-dependent nudging technique (Lin et al., 2012) is employed to relax the simulated winds and temperatures to reanalysis data, the nudging time scale is increased to 10 times that of the surface at 100 hPa and 100 times at 10 hPa. The nudging time scale at the surface is 6 hours. The simulation began on January 1, 1979, and ended on November 31, 2004. Then, it continued for four years with daily output. The analysis is based on the simulation's daily output from July 2005 to December 2010. The initial atmospheric state is derived from the ERA-Interim reanalysis.

In this instance, the e90 (an artificial tracer with uniform lifetime of 90 days in the atmosphere) tracer is employed to determine the tropopause (Prather et al., 2011). In the lowest model layer the e90 tracer is relaxed to 120 ppb over a timescale of 1 hours. The tropopause value of e90 is defined to be 72 ppb in this model through comparing with the thermal tropopause in the tropics.

2.2 Measurements and reanalysis

The High Resolution Dynamics Limb Sounder (HIRDLS) instrument measures infrared emission at 21 channels ranging from 6.12 to 17.76 microns in the upper troposphere, stratosphere and mesosphere (Gille et al., 2008). Profiles of O_3 and other atmospheric constituents, as well as cloud top pressure, were retrieved at a high vertical resolution of approximately 1 km from latitudes of -64 to 80 degrees. HIRDLS data collection began on January 21, 2005 and ended in early 2008. The high resolution of HIRDLS, spanning from the upper troposphere to the lower mesosphere, makes it an effective instrument for measuring fine atmospheric features in UTLS (the upper troposphere

https://doi.org/10.5194/egusphere-2026-3817
Preprint. Discussion started: 14 July 2026

and lower stratosphere), a region that most satellites cannot effectively measure. This study uses V7 Level 2 O_3 profiles above the cloud top.

Additionally, the EAC4 (ECMWF Atmospheric Composition Reanalysis 4) O_3 reanalysis is used to evaluate modeled stratospheric intrusions. EAC4 O_3 combines model data with observation from across the world into a globally complete and consistent dataset using data assimilation approach (Inness et al., 2019).

The model simulated tropospheric OH is evaluated against OH from EAC4 reanalysis and CCMI-2022 (the Chemistry Climate Model Initiative 2022) models. In EAC4 observations of OH precursors (O_3, NO_2) as well as CO are assimilated. Outputs from the CCMI-2022 REF-D1 experiments are used. The REF-D1 historical hindcast simulations cover the period 1960-2018 and use the observed historical forcings, including monthly mean SST and SIC, ozone-depleting substances (ODS) and long-lived greenhouse gases (GHG).

3 Results and Discussions

3.1 Evaluation of the model

Figure 1a, b, c show the HIRDLS measurements and the AM3 model simulations of O_3 profiles at different latitudes and along the HIRDLS orbit track on selected days. In the tropical bands (30° S-30° N), the modeled and measured profiles agree generally well, except for an overestimation of the maximum O_3 concentration at 10 hPa by about 7%. Above 10 hPa, the model underestimates the O_3 concentration by up to 300 ppb in the extratropics. In the lower stratosphere, the model presents an underestimation compared to the HIRDLS in the tropics and agrees well with the measurements in the extratropics. The underestimation in the tropics could be due to too strong deep convection in the model, which can quickly take ozone-poor air in the boundary layer into the upper troposphere.

Lin et al. (2012) and Lin et al. (2015) used the AM3 model to study the transport of O_3 from the stratosphere to the troposphere. These studies employed horizontal resolutions of 200×200 km^2 and 50×50 km^2. According to the model evaluation in Lin et al. (2015), both resolutions can reproduce the large-scale occurrence of deep stratospheric intrusions and their impact on the day-to-day variability of O_3 below 3 km. This study applied a horizontal resolution of 100×100 km^2, and it is expected that the model correctly captured stratospheric intrusions. Along the HIRDLS orbit track, the model captures variations in O_3 concentration due to changes in the tropopause and stratospheric intrusions (Fig. 1b and 1c). The high degree of similarity between the model simulations and the

https://doi.org/10.5194/egusphere-2026-3817
Preprint. Discussion started: 14 July 2026

measurements indicates that the model reasonably simulates the transport process of air mass from the stratosphere to the troposphere.

Figure 1d compares cross sections of the modeled and EAC4 O_3 along 100° E on selected days. Compared to EAC4 the model captures the tropopause fold and associated stratospheric O_3 descent in the extratropics. In the subtropics the model reasonably simulates tropopause fold events but underestimates the associated O_3 descent. Such underestimation could be due too strong deep convection in the model, which dilutes O_3 concentration in the tropical UTLS region. In the tropics there are frequent descent of stratospheric O_3 in EAC4 that is not simulated by the model well. However, it is less reliable that significant amount of stratospheric O_3 directly descends into the troposphere across the tropical tropopause.

(a)

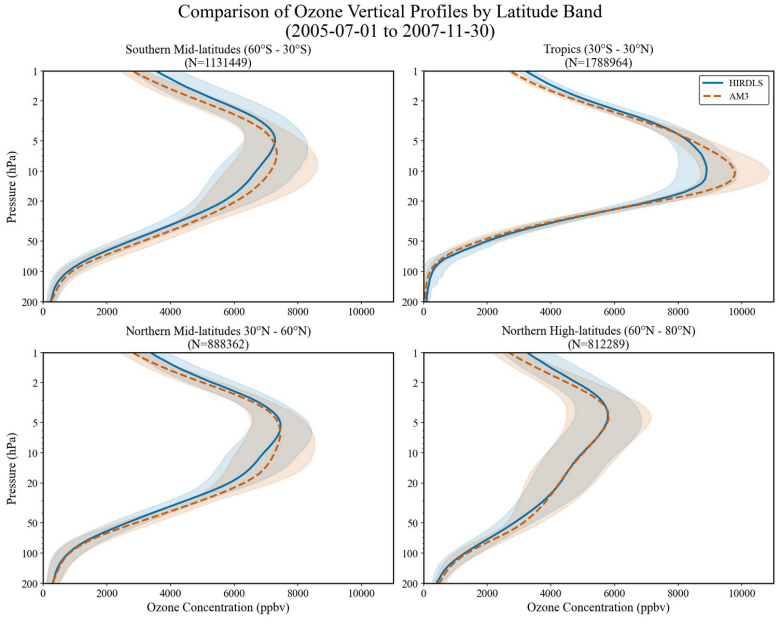

(b)

https://doi.org/10.5194/egusphere-2026-3817
Preprint. Discussion started: 14 July 2026

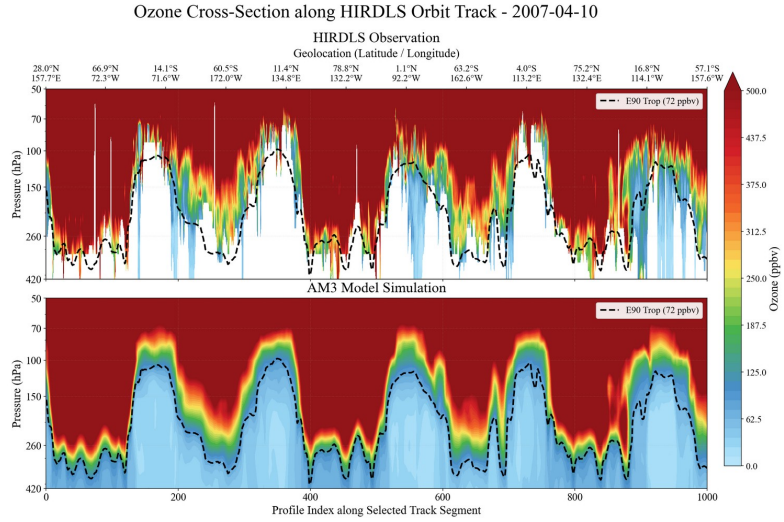

(c)

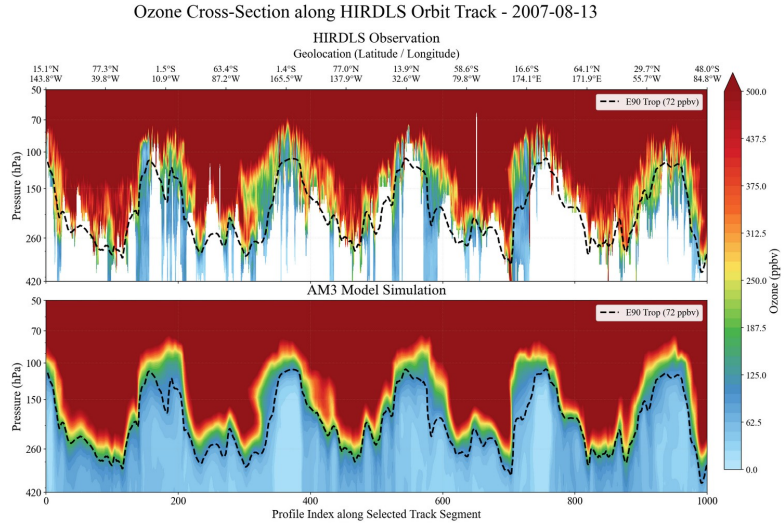

(d)

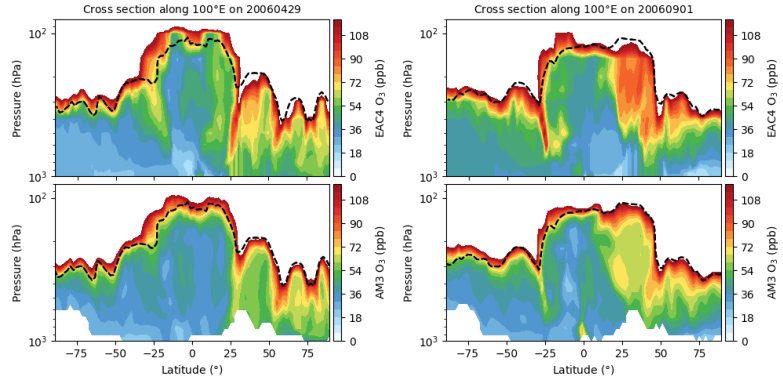

205

https://doi.org/10.5194/egusphere-2026-3817
Preprint. Discussion started: 14 July 2026

Figure 1. Comparison of the modeled and measured O_3 profiles in different latitude bands, averaged from July 2005 to November 2007 (a), and along the HIRDLS sampling orbit track on April 10 (b) and August 13, 2007 (c), as well as comparison between EAC4 and the modeled O_3 along 100 °E longitude on selected days (d). The black lines indicate the 72 ppb contour lines of the modeled e90.

Figure 2 shows the spatial distributions of volume-weighted tropospheric and zonal mean OH concentration of the AM3 model, EAC4 reanalysis and four CCMI-2022 models. Compared to the CCMI-2022 models the AM3 model simulates a tropospheric mean OH that is close to EAC4. However, over the tropical Africa and northern South America large differences occur between different models. In these regions, NO_x and NMVOCs emissions by tropical rainforest have significant influences on tropospheric OH, the CCMI-I models show large discrepancies as well (Zhao et al., 2019). The global mean mass-weighted tropospheric OH simulated by the AM3 model is 10.10×10^5 molec cm^{-3} during 2010, which is close to the observation-based value given in Zhao et al. (2023). In their simulation, the CO, NO_2, O_3, CH_4, and CH_2O, total column O_3, T_a and $H_2O_{(g)}$ are replaced with the available observation-based data. Considering the zonal mean OH concentration, the AM3 and CCMI-2022 models simulate a distribution that is more concentrated in the lower troposphere. In contrast, EAC4 shows a distribution that is more uniform in the vertical. A second maximum occurs in EAC4 OH concentration just below the tropical tropopause, which could be related to lightning NO_x emissions. The AM3 model show high similarity with CESM2-WACCM in the zonal mean distribution.

(a)

https://doi.org/10.5194/egusphere-2026-3817
Preprint. Discussion started: 14 July 2026

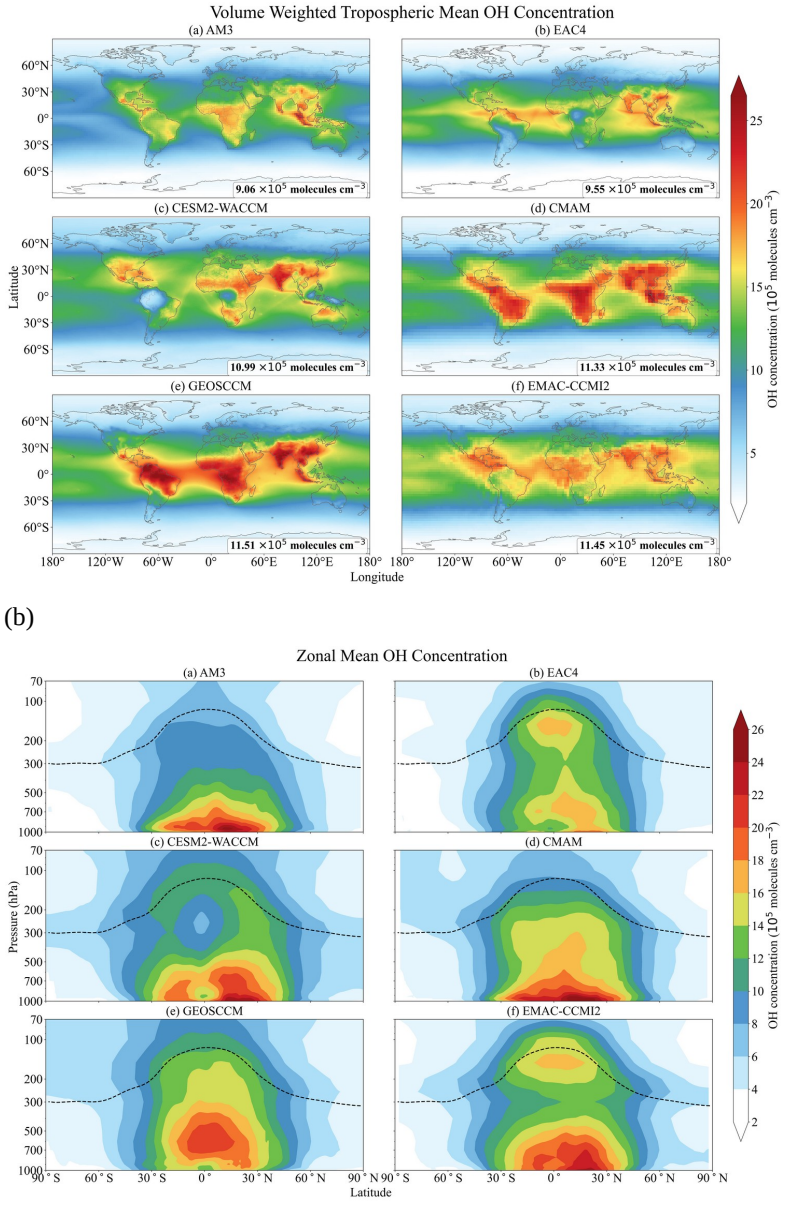

(b)

230 Figure 2. The spatial distributions of volume-weighted tropospheric mean (a) and zonal mean (b) OH concentration fields of AM3 and CCMI-2022 models and EAC4 reanalysis averaged for 2006-2010. Global mean values are shown as insets.

3.2 Monthly variations of StrOH in the troposphere

235 Figure 3 shows the monthly StrOH concentrations in the troposphere as simulated by the AM3 model and averaged over the period from January 2006 to December 2010. The spatial distribution

https://doi.org/10.5194/egusphere-2026-3817
Preprint. Discussion started: 14 July 2026

of StrOH at 400 hPa reveals higher StrOH concentrations in the summer subtropics. In the northern hemisphere, the highest concentrations occur over the subtropical Pacific at about 2×10^{-2} ppt, and over the Tibetan Plateau at around 3×10^{-2} ppt. In the southern hemisphere, the highest concentrations occur over the subtropical oceans at about 2×10^{-2} ppt. Stratospheric O_3 is transported into the troposphere via the Brewer-Dobson circulation, which is strongest in the winter hemisphere. The high StrOH concentrations in summer subtropics could be due to stronger solar radiation, greater water vapour, and warmer air. During the summer months, the subtropical jet stream is positioned at the northern edge of the Tibetan Plateau. Stratospheric intrusions along the jet frequently transport stratospheric O_3 to the troposphere over the Tibetan Plateau. Additionally, due to the heating of the plateau, the tropopause can reach as high as 70 hPa over there. This results in a lower stratospheric O_3 column and then strong ultraviolet radiation. These factors could result in high tropospheric StrOH concentrations over the Tibetan Plateau during these time. At the surface (Figure 3b), the highest StrOH concentration occurs over the Tibetan Plateau, South Africa and northern South America, as well as subtropical oceans.

At both 400 hPa and the surface, there are negative StrOH concentrations occur, e.g. at northern high latitudes, northern Africa, southern South America and South Africa. It means stratospheric intrusions result in decrease of tropospheric OH. In the troposphere, O_3 is a precursor of OH as well as a sink by reaction $O_3+OH\rightarrow HO_2+O_2$. HO_2 can be transformed back to OH trough reactions with NO and O_3. In addition, HO_2 can react with itself or RO_2 to form a final loss of HO_x (HO_2+OH). It is expected that in dry condition and low NO_x environment the sink effect of O_3 is more important than the source effect. In these cases, stratosphere intrusions possibly decrease tropospheric OH.

(a)

https://doi.org/10.5194/egusphere-2026-3817
Preprint. Discussion started: 14 July 2026

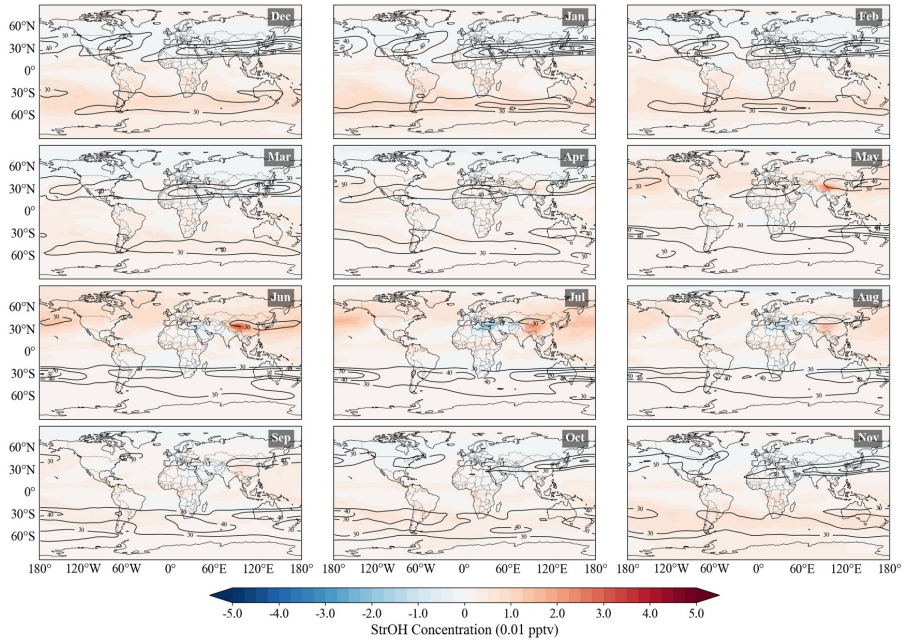

260 (b)

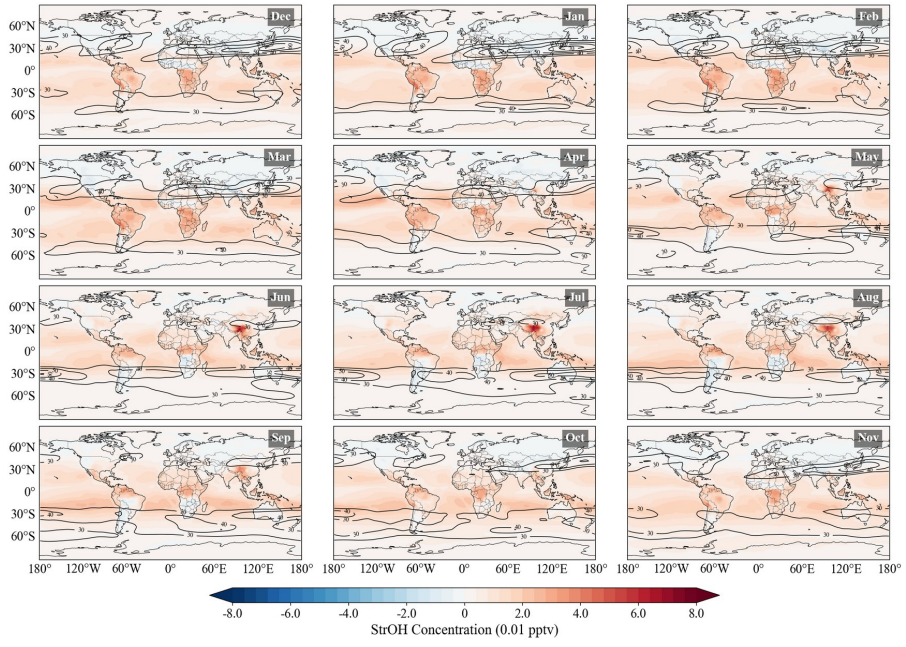

https://doi.org/10.5194/egusphere-2026-3817
Preprint. Discussion started: 14 July 2026

Figure 3. The Spatial distribution of the monthly averaged concentrations of StrOH at (a) 400 hPa and (b) the surface is shown for the period from 2006 to 2010. The black lines indicate zonal wind speed at 200 hPa.

3.3 Seasonal cycle of StrOH in the selected region

In this section, we select several regions for further analysis of StrOH production and loss. These regions are the Tibetan Plateau, the subtropical ocean, northern South America and South Africa. These regions are enclosed by boxes in Figure 4.

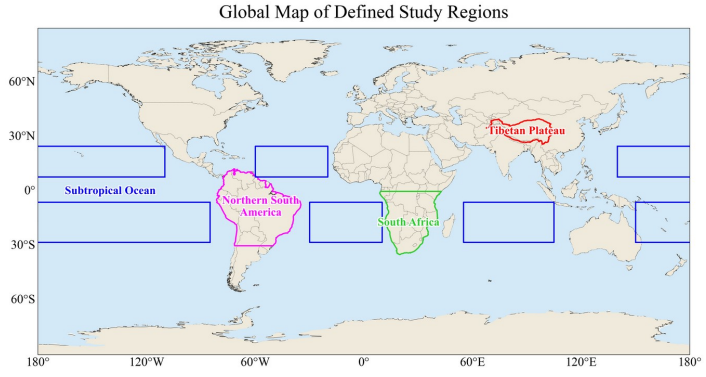

Figure 4. The regions selected for in-depth analysis.

Figure 5 shows the monthly variations in the production rate of StrOH through the $StrO_3$+hv and $StrO_3$+HO_2 reactions, as well as the loss rate constant, L(OH)/[OH], at the surface of Tibetan Plateau. These values are averaged from January 2006 to December 2010. Additionally, the concentrations of OH, StrOH, $StrO_3$, and specific humidity are displayed. At the Tibetan Plateau surface, StrOH concentrations reach their annual maximum in July and August, at approximately 5×10^{-2} ppt. The maximum StrOH concentration is due to the two production reactions, both of which are high in summer months. The first reaction, $StrO_3$+hv, contributes about 85% to the maximum StrOH concentration in this month. The relative contributions of StrOH to tropospheric OH peak at similar months (approximately 7.5%) and reach -11% in winter months. The negative contribution corresponds to weak ultraviolet radiation and dry condition in winter, which reduces the source effect of $StrO_3$.

The concentration of $StrO_3$ is highest in April and lowest in November in this region. This seasonal variation in $StrO_3$ is due to the Brewer-Dobson circulation (BDC), which transports O_3 produced in

https://doi.org/10.5194/egusphere-2026-3817
Preprint. Discussion started: 14 July 2026

the tropical middle stratosphere to higher latitudes. At these latitudes, O_3 is transported downward to the lower stratosphere. The northern branch of the BDC is strongest during the winter months, resulting in highest levels of $StrO_3$ in the spring. This time lag between the strongest BDC and the highest level of $StrO_3$ is due to the transport of O_3 from the lower stratosphere to the troposphere. Specific humidity exhibits a maximum in August and a minimum in January. These results in Figures 5 reveals that the seasonal variation of StrOH over the Tibetan Plateau is more impacted by solar radiation and specific humidity, due to its relative dry condition.

Figure 6 shows the monthly production rate of StrOH and the loss rate constant averaged over the subtropical ocean surface. In this region, seasonal variations of both OH and StrOH concentrations are not significant. StrOH concentrations vary between 1 and 2 $\times 10^{-2}$ ppt and with a relative contribution of approximately 22%. Similarly, the two production reactions also show insignificant seasonal changes with the first takes about 86%. In this region, StrOH does not show negative contributions, possibly due to high specific humidity (around 14 g/kg compared 1.5 g/kg in winter Tibetan Plateau).

Figure 7 shows the monthly production rate of StrOH and the loss rate constant, averaged over the surface of the northern South America. The maximum StrOH concentration is about 2.5×10^{-2} ppt, occurs in winter. The relative contribution of StrOH peak in winter as well, reaching approximately 13%. The first production reaction contributes about 80%. As explained in Section 3.1 the various models show large discrepancies in the volume-weighted tropospheric OH concentration over the northern South America, which ranges approximately from 5 to 25 $\times 10^{5}$ molec cm^{-3}. The AM3 model locates at the middle of this range. Therefore, the relative contribution of stratospheric intrusion could be doubled if taking EAC4 and CESM2-WACCM as the reference.

Figure 8 shows the monthly production rate of StrOH and the loss rate constant, averaged over the surface of South Africa. Similar to the northern South America, the maximum StrOH concentration in this region is about 2.5×10^{-2} ppt, occurs in winter. The maximum StrO3 concentration as well as loss rate constant occur in summer when StrOH and specific humidity reach their minima. Considering relative high specific humidity through the year, approximately above 8 g/kg, it is speculated that StrOH in this region is controlled mostly by OH sink strength. The relative contribution of stratospheric intrusions ranges from -1% to 12%.

https://doi.org/10.5194/egusphere-2026-3817
Preprint. Discussion started: 14 July 2026

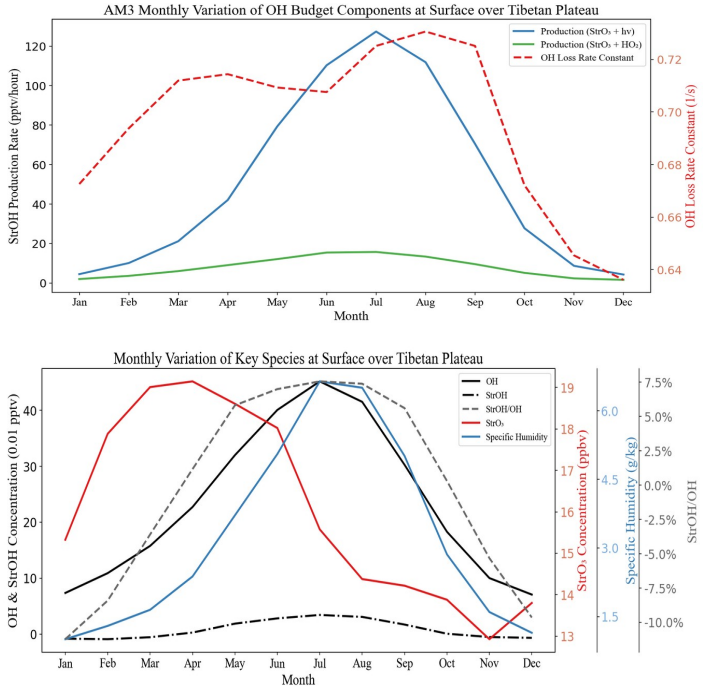

Figure 5. Monthly variations of StrOH production rates, loss rate constant (L(OH)/[OH]) and related species averaged in the period 2006-2010 and over the Tibetan Plateau surface.

320

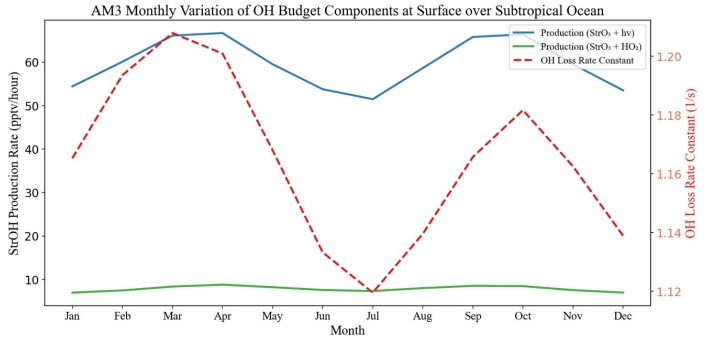

https://doi.org/10.5194/egusphere-2026-3817
Preprint. Discussion started: 14 July 2026

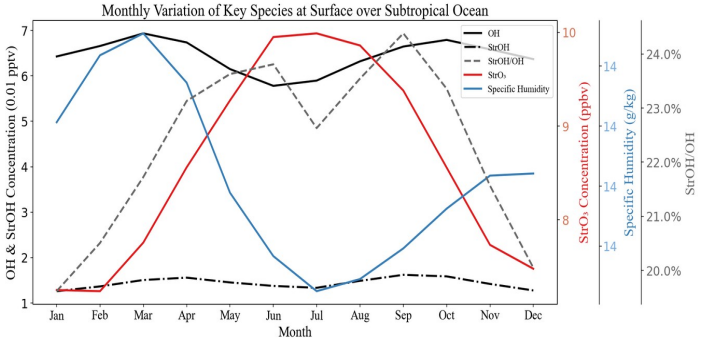

Figure 6. Monthly variations of StrOH production rates and loss rate constant (L(OH)/[OH]) and related species averaged in the period 2006-2010 and over the surface of subtropical ocean.

325

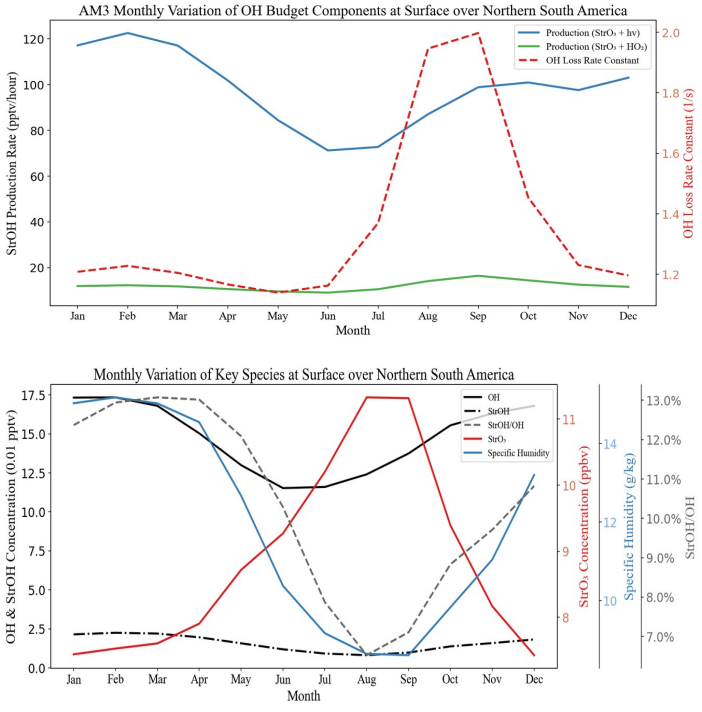

Figure 7. Monthly variations of StrOH production rates and loss rate constant (L(OH)/[OH]) and related species averaged in the period 2006-2010 and over the surface of the northern South

330 America.

https://doi.org/10.5194/egusphere-2026-3817
Preprint. Discussion started: 14 July 2026

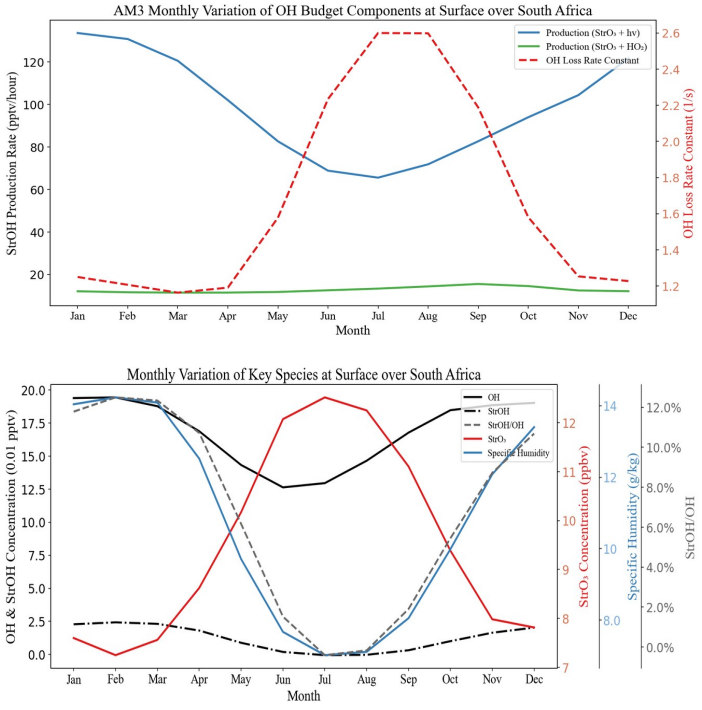

Figure 8. Monthly variations of StrOH production rates and loss rate constant (L(OH)/[OH]) and related species averaged in the period 2006-2010 and over the surface of South Africa.

4 Conclusions and discussion

In this study, the investigation focuses on the contribution of stratospheric intrusion to tropospheric OH. This investigation is conducted through the utilization of a chemistry-climate model for the period from 2006 to 2010.

4.1 StrOH in the troposphere

In the middle troposphere (400 hPa), the result reveals that the stratospheric contribution is high in the summer subtropics, reaching 2×10^{-2} ppt over the subtropical Pacific and 3×10^{-2} ppt over the Tibetan Plateau. At the surface, the spatial distributions of StrOH are similar to those at 400 hPa except for with increased amount. In some months negative StrOH concentrations occur in some regions, for example at the northern high latitudes, northern Africa, southern South America and South Africa. It means stratospheric intrusions can result in decreases in tropospheric OH even if they result in the downward transport of higher concentrations of ozone.

A detailed analysis of the mechanism in selected regions reveals that stratospheric contributions to tropospheric OH primarily occur through the photolysis of stratospheric O_3 (above 80%

https://doi.org/10.5194/egusphere-2026-3817
Preprint. Discussion started: 14 July 2026

contribution) and, secondarily, through reaction with HO_2. Several factors influence the seasonal variation of the stratospheric contribution, including stratospheric O_3, specific humidity, and solar radiation. When the primary production of tropospheric OH is inhibited by dry condition or weak ultraviolet radiation negative StrOH concentrations occur. In this case intrusions of stratospheric O_3 mostly increase sink of tropospheric OH, e.g. the winter Tibetan Plateau.

Considering relative contributions of stratospheric intrusions at the surface, subtropical ocean regions show highest influences of around 22%. The relative contributions range from -11% to 7.5% over the Tibetan Plateau surface, from 6% to 13% over the surface of northern South America and from -1% to 12% over the surface of South Africa.

4.2 Discussion

Previous studies have revealed significant modulation of air pollution and lightning NO_x emissions on trends and variability of the tropospheric OH (Turner et al., 2018; Zhao et al., 2025). The results in this study indicate that stratospheric ozone intrusion has important contribution to the tropospheric OH as well, particularly near the surface. The downward transport of stratospheric ozone are influenced by the BDC strength and stratospheric ozone recovery, both of which are expected to increase stratospheric contribution to tropospheric ozone in the future. Wang et al. (2023) estimated an increase in ozone STE (stratosphere-troposphere exchange) of 4.7% per decade for the period 2000-2099. In CMIP6 models the net chemical production of tropospheric ozone ranges from 411 (266) to 839 (675) Tg yr^{-1} and STE of ozone ranges from 481 (692) to 28 (212) Tg yr^{-1} around 2000 (2095) (Griffiths et al., 2021). Three out of four CMIP6 models show a turning point when the net chemical production become less than ozone STE around 2010. Hence, it is expected that the primary production of tropospheric OH will be increasingly controlled by the stratospheric ozone transported via STE in the future.

There are many internal forcing factors that can result in interannual variability of the ozone STE. The important factors include sea surface temperature (SST) variations in the tropical eastern Pacific, the Pacific warm pool region, and quasi-biennial oscillation in the tropical stratospheric wind (QBO) (Xie et al., 2017; Zhang et al., 2025). Additionally, the frequency and strength of these forcing factors present long-term trends due to external forcing, such as greenhouse gas emissions. By analyzing CMIP6 models Erickson and Patricola (2023) concluded that SST in the tropical eastern Pacific will shifts toward a more warm anomalies condition. The warm anomaly tends to strengthens downward transport of extratropical stratosphere ozone. In contrast, the QBO is projected to become weaker under global warming (Luo et al., 2026). These signals are possibly

https://doi.org/10.5194/egusphere-2026-3817
Preprint. Discussion started: 14 July 2026

reflected in the interannual variability of tropospheric OH, particularly in the future when STE of ozone play a more important role in budget of tropospheric ozone.

One important uncertainty of our results concerns the downward transport of stratospheric O_3. In Figure 1d, the AM3 simulation shows weaker downward intrusion of stratospheric O_3 than EAC4. If EAC4 is correct, then the contribution to tropospheric OH from stratospheric intrusion could be underestimated. Basically stratospheric intrusion is a mesoscale process and is difficult for a global model to capture. The second uncertainty arises from the chemistry of OH production and loss, particularly that associated with isoprene oxidation. Regeneration of OH in the photochemistry of isoprene is important in the tropical rainforest region, where it significantly affects the abundances of OH. This process is complex and still not completely understood (Bates and Jacob, 2019). Correspondingly, the AM3 and CCMI-2022 models show significant differences in the tropical parts of South American and Africa.

Data availability

The HIRDLS V7 O_3 profiles are available at https://search.earthdata.nasa.gov/search/granules?p=C1251101072-GES_DISC&pg[0][v]=f&pg[0][gsk]=-start_date&fi=HIRDLS&fl=2%2B-%2BGeophys.%2BVariables%252C%2BSensor%2BCoordinates&tl=1156377600!4!!&fsm0=Atmospheric+Chemistry&fst0=Atmosphere&fpb0=Space-based+Platforms. The AM3 model code is freely available at https://www.gfdl.noaa.gov/am3/. The CCMI-2022 outputs are available from the Centre for Environmental Data Analysis (CEDA). The EAC4 reanalysis data is publicly available at https://ads.atmosphere.copernicus.eu/datasets/cams-global-reanalysis-eac4?tab=download.

Author contributions

The paper was designed and written by ZW. YZ and XH perform model outputs analysis and visualization. All co-authors actively contributed to the extended discussions, refinement of the study design.

Conflicts of interest

The authors state that they do not have any conflicts of interest.

Acknowledgments

We acknowledge the HIRDLS team for proving ozone profiles and NOAA GFDL team for providing AM3 code. We acknowledge the modeling groups for making their simulations available for this analysis, the joint WCRP SPARC/IGAC Chemistry-Climate Model Initiative (CCMI) for

https://doi.org/10.5194/egusphere-2026-3817
Preprint. Discussion started: 14 July 2026

organizing and coordinating the model data analysis activity, and the Centre for Environmental Data Analysis (CEDA) for collecting and archiving the CCMI model output.

Financial support

This research is sponsored by the National Natural Science Foundation of China (NSFC) General Projects 42275072 and jointly supported by the Project supported by the Joint Fund of the National Natural Science Foundation of China and the China Meteorological Administration (U2442211).

References

Brauers, T., Dorn,H.-P., Koch, H., Kraus, A. B., and Plass-Dülmer, C. (1998). Meteorological aspects, ozone, and solar radiation measurements during POPCORN 1994, *J. Atmos. Chem.*, 31, 33–52.

Bates, K. H., & Jacob, D. J. (2019). A new model mechanism for atmospheric oxidation of isoprene: global effects on oxidants, nitrogen oxides, organic products, and secondary organic aerosol. *Atmospheric Chemistry and Physics*, *19*(14), 9613–9640. https://doi.org/10.5194/acp-19-9613-2019

Cui, Z., Zhang, G. J., Wang, Y., & Xie, S. (2021). Understanding the roles of convective trigger functions in the diurnal cycle of precipitation in the NCAR CAM5. *Journal of Climate*, *34*(15), 6473–6489. https://doi.org/10.1175/jcli-d-20-0699.1

Divakarla, M., Barnet, C., Goldberg, M., Maddy, E., Irion, F., Newchurch, M., Liu, X., Wolf, W., Flynn, L., Labow, G., Xiong, X., Wei, J., & Zhou, L. (2008). Evaluation of Atmospheric Infrared Sounder ozone profiles and total ozone retrievals with matched ozonesonde measurements, ECMWF ozone data, and Ozone Monitoring Instrument retrievals. *Journal of Geophysical Research Atmospheres*, *113*(D15). https://doi.org/10.1029/2007jd009317

Donner, L. J., Wyman, B. L., Hemler, R. S., Horowitz, L. W., Ming, Y., Zhao, M., Golaz, J., Ginoux, P., Lin, S., Schwarzkopf, M. D., Austin, J., Alaka, G., Cooke, W. F., Delworth, T. L., Freidenreich, S. M., Gordon, C. T., Griffies, S. M., Held, I. M., Hurlin, W. J., . . . Zeng, F. (2011). The dynamical core, physical parameterizations, and basic simulation characteristics of the atmospheric component AM3 of the GFDL Global Coupled Model CM3. *Journal of Climate*, *24*(13), 3484–3519. https://doi.org/10.1175/2011jcli3955.1

Esler, J. G., Tan, D. G., Haynes, P. H., Evans, M. J., Law, K. S., Plantevin, P., & Pyle, J. A. (2001). Stratosphere-Troposphere Exchange: Chemical sensitivity to mixing. *Journal of Geophysical Research: Atmospheres*, *106*(D5), 4717–4731. https://doi.org/10.1029/2000jd900405

https://doi.org/10.5194/egusphere-2026-3817
Preprint. Discussion started: 14 July 2026

Erickson, N. E., & Patricola, C. M. (2023). Future projections of the El Niño-Southern Oscillation and Tropical Pacific Mean State in CMIP6. *Journal of Geophysical Research Atmospheres*, *128*(21). https://doi.org/10.1029/2022jd037563

Gille, J. C., and L. J. Gray (2011), High Resolution Dynamics Limb Sounder Earth Observing System (EOS) data description and quality, *Tech. Rep*. [Available at http://www.eos.ucar.edu/hirdls/data/products/HIRDLS-DQD-V6-1.pdf.]

Inness, A., Ades, M., Agustí-Panareda, A., Barré, J., Benedictow, A., Blechschmidt, A.-M., Dominguez, J. J., Engelen, R., Eskes, H., Flemming, J., Huijnen, V., Jones, L., Kipling, Z., Massart, S., Parrington, M., Peuch, V.-H., Razinger, M., Remy, S., Schulz, M., and Suttie, M. (2019). The CAMS reanalysis of atmospheric composition, *Atmospheric Chemistry and Physics*, *19*(6), 3515–3556, https://doi.org/10.5194/acp-19-3515-2019

Kentarchos, A. S., & Roelofs, G. J. (2003). A model study of stratospheric ozone in the troposphere and its contribution to tropospheric oh formation. *Journal of Geophysical Research: Atmospheres*, *108*(D12). https://doi.org/10.1029/2002jd002598

Levy, H. (1971). Normal atmosphere: large radical and formaldehyde concentrations predicted. *Science*, *173*(3992), 141–143. https://doi.org/10.1126/science.173.3992.141

Lelieveld, J., Gromov, S., Pozzer, A., & Taraborrelli, D. (2016). Global tropospheric hydroxyl distribution, budget and reactivity. *Atmospheric Chemistry and Physics*, *16*(19), 12477–12493. https://doi.org/10.5194/acp-16-12477-2016

Lin, S. (2004). A "Vertically lagrangian" Finite-Volume dynamical core for global models. *Monthly Weather Review*, *132*(10), 2293–2307. https://doi.org/10.1175/1520-0493(2004)132

Lin, M., Fiore, A. M., Cooper, O. R., Horowitz, L. W., Langford, A. O., Levy, H., Johnson, B. J., Naik, V., Oltmans, S. J., & Senff, C. J. (2012). Springtime high surface ozone events over the western United States: Quantifying the role of stratospheric intrusions. *Journal of Geophysical Research Atmospheres*, *117*(D21). https://doi.org/10.1029/2012jd018151

Lin, M., Fiore, A. M., Horowitz, L. W., Langford, A. O., Oltmans, S. J., Tarasick, D., & Rieder, H. E. (2015). Climate variability modulates western US ozone air quality in spring via deep stratospheric intrusions. *Nature Communications*, *6*(1), 51–69. https://doi.org/10.1038/ncomms8105

Luo, F., Xie, F., Zhou, T., Niu, Y., Xia, Y., Luo, J., Zhang, R., Wang, Y., Liang, W., & Tian, W. (2026). The disappearing quasi-biennial oscillation under sustained global warming. *Nature Communications*, *17*(1). https://doi.org/10.1038/s41467-026-68922-2

https://doi.org/10.5194/egusphere-2026-3817
Preprint. Discussion started: 14 July 2026

Montzka, S. A., Krol, M., Dlugokencky, E., Hall, B., Jöckel, P., & Lelieveld, J. (2011). Small interannual variability of global atmospheric hydroxyl. *Science*, *331*(6013), 67–69. https://doi.org/10.1126/science.1197640

Mao, J., Fan, S., Jacob, D. J., & Travis, K. R. (2013). Radical loss in the atmosphere from Cu-Fe redox coupling in aerosols. *Atmospheric Chemistry and Physics*, *13*(2), 509–519. https://doi.org/10.5194/acp-13-509-2013

Mao, J., Horowitz, L. W., Naik, V., Fan, S., Liu, J., & Fiore, A. M. (2013). Sensitivity of tropospheric oxidants to biomass burning emissions: implications for radiative forcing. *Geophysical Research Letters*, *40*(6), 1241–1246. https://doi.org/10.1002/grl.50210

Nicely, J. M., Canty, T. P., Manyin, M., Oman, L. D., Salawitch, R. J., Steenrod, S. D., Strahan, S. E., & Strode, S. A. (2018). Changes in global tropospheric OH expected as a result of climate change over the last several decades. *Journal of Geophysical Research Atmospheres*, *123*(18). https://doi.org/10.1029/2018jd028388

Nicely, J. M., Duncan, B. N., Hanisco, T. F., Wolfe, G. M., Salawitch, R. J., Deushi, M., Haslerud, A. S., Jöckel, P., Josse, B., Kinnison, D. E., Klekociuk, A., Manyin, M. E., Marécal, V., Morgenstern, O., Murray, L. T., Myhre, G., Oman, L. D., Pitari, G., Pozzer, A., . . . Zeng, G. (2020). A machine learning examination of hydroxyl radical differences among model simulations for CCMI-1. *Atmospheric Chemistry and Physics*, *20*(3), 1341–1361. https://doi.org/10.5194/acp-20-1341-2020

Naik, V., Horowitz, L. W., Fiore, A. M., Ginoux, P., Mao, J., Aghedo, A. M., & Levy, H. (2013). Impact of preindustrial to present-day changes in short-lived pollutant emissions on atmospheric composition and climate forcing. *Journal of Geophysical Research: Atmospheres*, 118, 8086–8110. https://doi.org/10.1002/jgrd.50608

Patra, P. K., Krol, M. C., Prinn, R. G., Takigawa, M., Mühle, J., Montzka, S. A., Lal, S., Yamashita, Y., Naus, S., Chandra, N., Weiss, R. F., Krummel, P. B., Fraser, P. J., O'Doherty, S., & Elkins, J. W. (2020). Methyl chloroform continues to constrain the hydroxyl (OH) variability in the troposphere. *Journal of Geophysical Research Atmospheres*, *126*(4). https://doi.org/10.1029/2020jd033862

Pittman, J. V., Pan, L. L., Wei, J. C., Irion, F. W., Liu, X., Maddy, E. S., Barnet, C. D., Chance, K., & Gao, R. (2009). Evaluation of AIRS, IASI, and OMI ozone profile retrievals in the extratropical tropopause region using in situ aircraft measurements. *Journal of Geophysical Research Atmospheres*, *114*(D24). https://doi.org/10.1029/2009jd012493

https://doi.org/10.5194/egusphere-2026-3817
Preprint. Discussion started: 14 July 2026

Putman, W. M., & Lin, S. (2007). Finite-volume transport on various cubed-sphere grids. *Journal of Computational Physics*, 227(1), 55–78. https://doi.org/10.1016/j.jcp.2007.07.022

Rigby, M., Montzka, S. A., Prinn, R. G., White, J. W. C., Young, D., O'Doherty, S., Lunt, M. F., Ganesan, A. L., Manning, A. J., Simmonds, P. G., Salameh, P. K., Harth, C. M., Mühle, J., Weiss, R. F., Fraser, P. J., Steele, L. P., Krummel, P. B., McCulloch, A., & Park, S. (2017). Role of atmospheric oxidation in recent methane growth. *Proceedings of the National Academy of Sciences*, *114*(21), 5373–5377. https://doi.org/10.1073/pnas.1616426114

Rowlinson, M. J., Rap, A., Arnold, S. R., Pope, R. J., Chipperfield, M. P., McNorton, J., Forster, P., Gordon, H., Pringle, K. J., Feng, W., Kerridge, B. J., Latter, B. L., and Siddans, R. (2019). Impact of El Niño–Southern Oscillation on the interannual variability of methane and tropospheric ozone, *Atmos. Chem. Phys.*, *19*, 8669–8686. https://doi.org/10.5194/acp-19-8669-2019

Spivakovsky, C. M., Logan, J. A., Montzka, S. A., Balkanski, Y. J., Foreman-Fowler, M., Jones, D. B. A., Horowitz, L. W., Fusco, A. C., Brenninkmeijer, C. a. M., Prather, M. J., Wofsy, S. C., & McElroy, M. B. (2000). Three-dimensional climatological distribution of tropospheric OH: Update and evaluation. *Journal of Geophysical Research Atmospheres*, *105*(D7), 8931–8980. https://doi.org/10.1029/1999jd901006

Suhas, E., & Zhang, G. J. (2014). Evaluation of trigger functions for convective parameterization schemes using observations. *Journal of Climate*, *27*(20), 7647–7666. https://doi.org/10.1175/jcli-d-13-00718.1

Tilmes, S., Lamarque, J., Emmons, L. K., Kinnison, D. E., Marsh, D., Garcia, R. R., Smith, A. K., Neely, R. R., Conley, A., Vitt, F., Martin, M. V., Tanimoto, H., Simpson, I., Blake, D. R., & Blake, N. (2016). Representation of the Community Earth System Model (CESM1) CAM4-chem within the Chemistry-Climate Model Initiative (CCMI). *Geoscientific Model Development*, *9*(5), 1853–1890. https://doi.org/10.5194/gmd-9-1853-2016

Turner, A. J., Frankenberg, C., Wennberg, P. O., & Jacob, D. J. (2017). Ambiguity in the causes for decadal trends in atmospheric methane and hydroxyl. *Proceedings of the National Academy of Sciences*, *114*(21), 5367–5372. https://doi.org/10.1073/pnas.1616020114

Turner, A. J., Fung, I., Naik, V., Horowitz, L. W., and Cohen, R. C. (2018). Modulation of hydroxyl variability by ENSO in the absence of external forcing, *Proceedings of the National Academy of Sciences*, *115*, 8931–8936. https://doi.org/10.1073/pnas.1807532115

https://doi.org/10.5194/egusphere-2026-3817
Preprint. Discussion started: 14 July 2026

Xie, F., Zhou, X., Li, J., Chen, Q., Zhang, J., Li, Y., Ding, R., Xue, J., & Ma, X. (2017). Effect of the Indo-Pacific Warm Pool on Lower-Stratospheric Water Vapor and Comparison with the Effect of ENSO. *Journal of Climate*, *31*(3), 929–943. https://doi.org/10.1175/jcli-d-17-0575.1

Xie, S., Wang, Y., Lin, W., Ma, H., Tang, Q., Tang, S., Zheng, X., Golaz, J., Zhang, G. J., & Zhang, M. (2019). Improved diurnal cycle of precipitation in E3SM with a revised convective triggering function. *Journal of Advances in Modeling Earth Systems*, *11*(7), 2290–2310. https://doi.org/10.1029/2019ms001702

Zhao, Y., Saunois, M., Bousquet, P., Lin, X., Berchet, A., Hegglin, M. I., Canadell, J. G., Jackson, R. B., Hauglustaine, D. A., Szopa, S., Stavert, A. R., Abraham, N. L., Archibald, A. T., Bekki, S., Deushi, M., Jöckel, P., Josse, B., Kinnison, D., Kirner, O., . . . Zheng, B. (2019). Inter-model comparison of global hydroxyl radical (OH) distributions and their impact on atmospheric methane over the 2000–2016 period. *Atmospheric Chemistry and Physics*, *19*(21), 13701–13723. https://doi.org/10.5194/acp-19-13701-2019

Zhao, Y., Saunois, M., Bousquet, P., Lin, X., Hegglin, M. I., Canadell, J. G., Jackson, R. B., and Zheng, B. (2023). Reconciling the bottom-up and top-down estimates of the methane chemical sink using multiple observations. *Atmospheric Chemistry and Physics*, 23, 789–807. https://doi.org/10.5194/acp-23-789-2023

Zhao, Y., Zheng, B., Saunois, M., Ciais, P., Hegglin, M. I., Lu, S., Li, Y., & Bousquet, P. (2025). Air pollution modulates trends and variability of the global methane budget. *Nature*, 642(8067), 369–375. https://doi.org/10.1038/s41586-025-09004-z

Zhang, Z., Wang, Z., Liang, J., & Luo, J. (2025). Impacts of the Quasi-Biennial oscillation and the El Niño-Southern oscillation on Stratosphere-to-Troposphere ozone Transport: Assessment with Chemistry-Climate Models. *Journal of Geophysical Research Atmospheres*, *130*(6). https://doi.org/10.1029/2024jd041825

Wang, M., & Fu, Q. (2023). Changes in Stratosphere-Troposphere exchange of air mass and ozone concentration in CCMI models from 1960 to 2099. *Journal of Geophysical Research Atmospheres*, *128*(13). https://doi.org/10.1029/2023jd038487